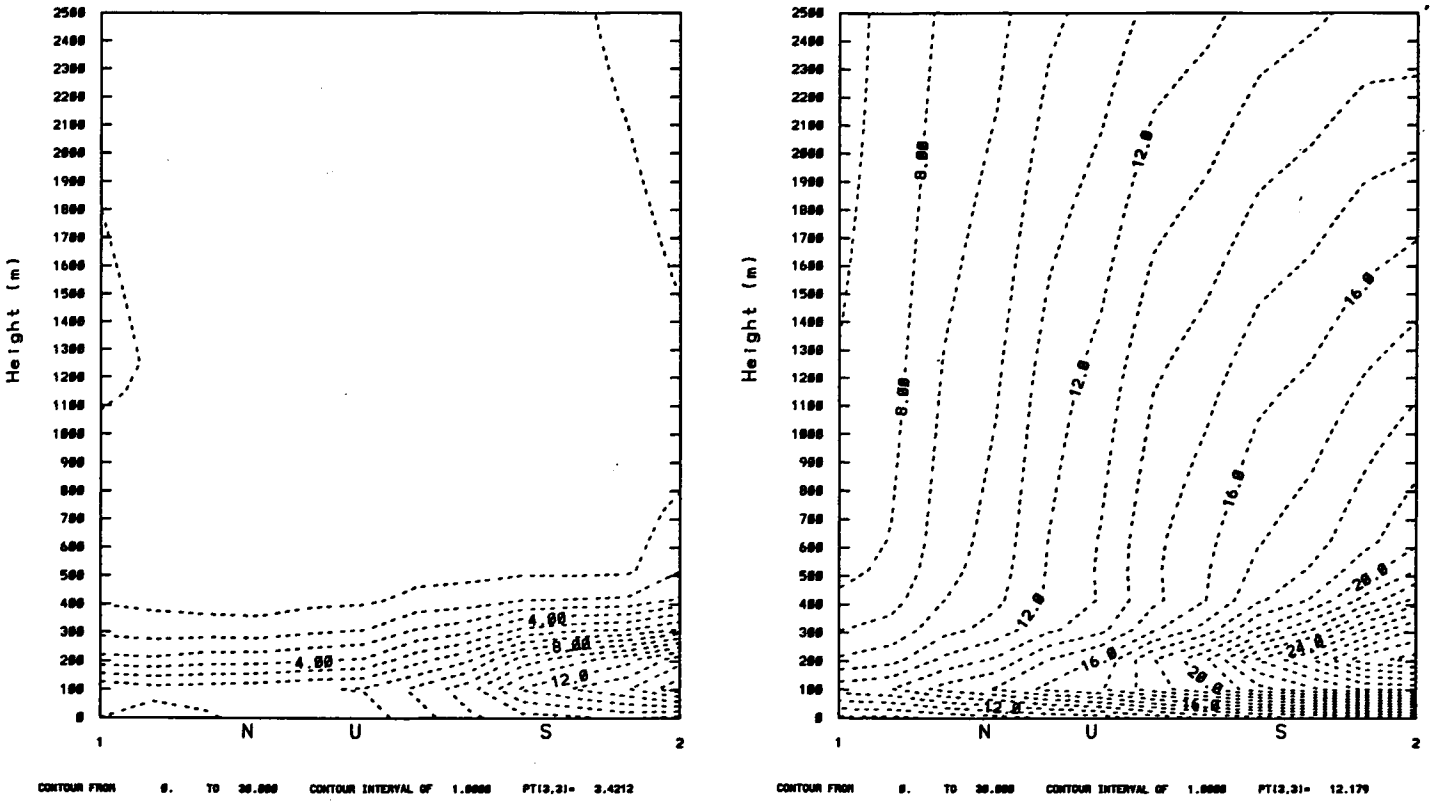

Figure 3. Vertical wind-speed cross sections along the three camps. *(Left)* For initial state of rest and *(right)* for initially prescribed pressure field.

main factor locating the strongest part of the confluence zone. This is important in understanding the highly irregular wind pattern over the antarctic continent. Qualitatively, the location of the simulated confluence zone is very consistent with the observed wind data.

This research was supported by National Science Foundation grant DPP 89-16921 to D. H. Bromwich. T. R. Parish provided valuable assistance with the modeling. The simulations were performed on the CRAY Y-MP of the Ohio Supercomputer Center, which is supported by the State of Ohio.

References

Ball, F. K. 1960. Winds on the ice slopes of Antarctica. *Antarctic Meteorology, Proceedings of the Symposium,* Melbourne, 1959. New York: Pergamon, 9-16.

Bromwich, D. H. 1986. Surface winds in West Antarctica. *Antarctic Journal of the U.S.*, 21(5):235-237.

Bromwich, D. H., J. F. Carrasco, and C. R. Stearns. 1992. Satellite observations of katabatic wind propagation for great distances across the Ross Ice Shelf. *Monthly Weather Review,* 120:1,940-1,949.

Bromwich, D. H. and Y. Du. 1991. Numerical simulation of the katabatic winds over West Antarctica. *Antarctic Journal of the U.S.*, 26(5):261-264.

Cerni, T. A. and T. R. Parish. 1984. A radiative model of the stable nocturnal boundary layer with application to the polar night. *Journal of Climate and Applied Meteorology,* 23:1,563-1,672.

Drewry, D. J. 1983. The surface of the antarctic ice sheet. In D. J. Drewry (Ed.), *Antarctica: Glaciological and Geophysical Folio, Sheet* 2. Cambridge, England: Scott Polar Research Institute.

Parish, T. R. 1981. The katabatic winds of Cape Denison and Port Martin. *Polar Record,* 20:525-532.

Parish, T. R. and D. H. Bromwich. 1987. The surface windfield over the antarctic ice sheets. *Nature,* 328:51-54.

Parish, T. R. and K. T. Waight. 1987. The forcing of antarctic katabatic winds. *Monthly Weather Review,* 115:2,214-2,226.

Schwerdtfeger, W. 1970. The climate of the Antarctic, Vol. 14. In S. Orvig, (Ed.) *World Survey of Climatology,* H. E. Landsberg, E., Elsevier, 253-355.

Photopolarimetry of halos and ice-crystal sizing

G. P. KÖNNEN

Royal Netherlands Meteorological Institute
De Bilt, The Netherlands

During nearby displays I recorded the linear polarization and intensity distributions of halos and simultaneously made replicas of the halo-generating ice crystals. My purpose was to explore halopolarimetry as a tool of remote sensing for crystals and to relate the diffraction broadening of the halo polarization and intensity directly with the sizes of the collected crystals.

I obtained polarization and intensity distributions of halos by means of the portable, four-lens monochromatic polarimetric camera (Können and Tinbergen 1991) shown in figure 1. This

Figure 1. I used this four-lens polarimetric camera to measure polarization and intensity distribution of halos.

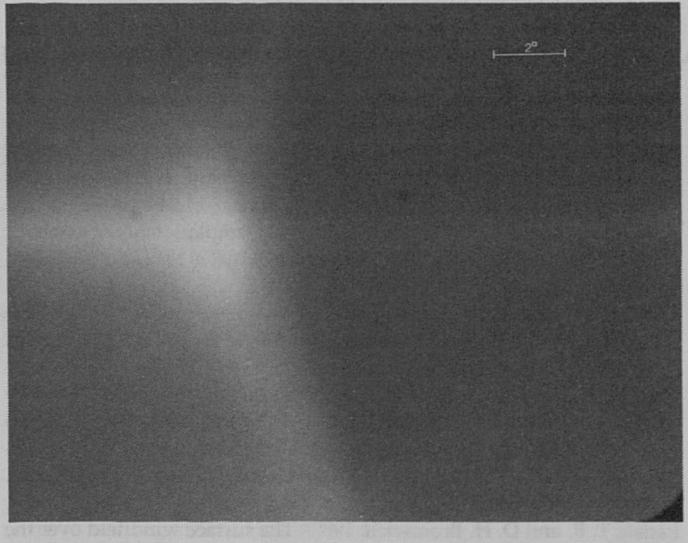

Figure 2. Diffraction-broadened parhelion, recorded on 1 January 1990 at 1403 Universal Time at Amundsen-Scott South Pole Station.

camera is a rebuilt commercial camera for passport photographs of 125-millimeter focal length. It takes four pictures simultaneously on one single Kodak Tri-X sheet film negative. Behind each lens is a polarizer, cut from the same sheet and with their orientations increasing in steps of 45°. The light then passes a filter with maximum transmission at 590-nanometer wavelength and 33-nanometer full width at half maximum. The negatives were digitized with a densitometer at a resolution of 50 x 50 micrometers. After conversion from density to intensity, the intensities in the pixels of the four images corresponding to the same area of sky were compared. The sum of the intensity of the pixels in two orthogonally polarized images provides the intensity I; its difference in the two pairs of orthogonally polarized images provides the second Stokes parameter Q and the third Stokes parameter U, respectively. The camera has a spirit level and a sun finder; if the sun is centered in that finder, the scattering angle in the images is known to within an accuracy of about 0.2°.

Figure 2 shows one of the four polarimetric images of a bright parhelion, taken on 1 January 1990 at 1403 Universal Time at Amundsen-Scott South Pole Station. The solar elevation was 23°. Figure 3 shows the intensity I and second Stokes parameter Q as a function of scattering angle, obtained from two of the four images on the digitized negative. Figure 3 passes straight through the intensity maximum of the parhelion. The plane of reference of the Stokes parameters is the horizontal, which closely coincides with the scattering plane. In the third Stokes parameter (not shown), the halo is not apparent so that the positive signal in Q indicates that the halo polarization is essentially horizontal. The degree of polarization equals Q/I. Note that the peak in Q occurs at a smaller scattering angle than does the halo intensity peak.

The parhelion polarization arises as follows (Können and Tinbergen 1991): After the entrance in the birefringent ice crystal, the light splits up into two polarized beams, each of them producing its own parhelion. Since the index of refraction is slightly different, the scattering angle domains of the two polarized parhelia are slightly shifted. In the region where the parhelion intensity changes rapidly with scattering angle, one of the polarized components predominates. The steepest part of the intensity distribution is near the geometrical parhelion scattering angle; hence, this is the region where strongest polarization is observed (see figure 3). Visually, the parhelion polarization manifested itself clearly as a 0.1° shift in halo position when viewed through rotating polarizer.

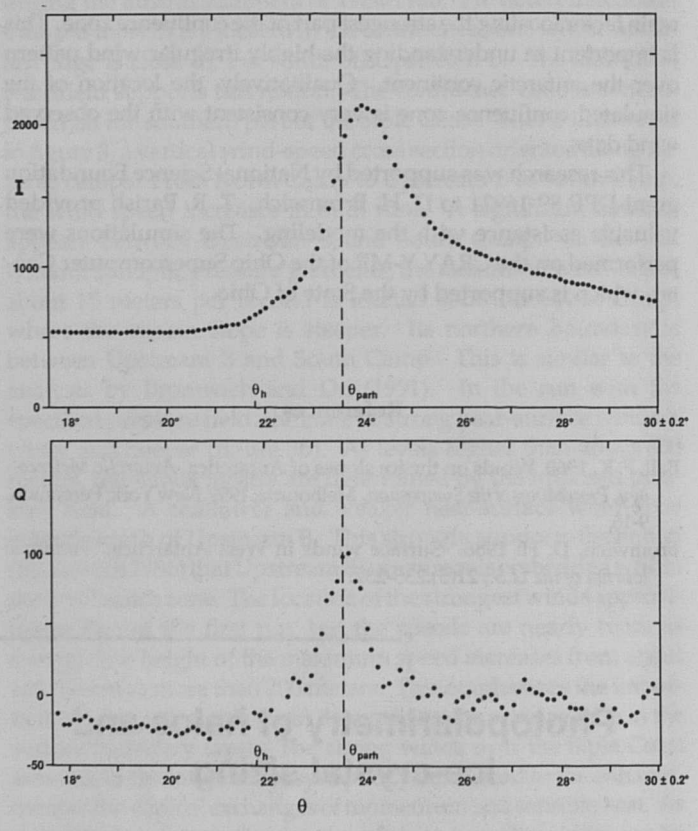

Figure 3. Intensity *I* and second Stokes parameter *Q* of the parhelion of figure 2 as a function of scattering angle θ. The 22° halo angle (random crystal orientation) and the parhelion scattering angle (preferential orientation) are denoted by θ_h and θ_{parh}, respectively. Q>0 indicates horizontal polarization; Q/I is degree of polarization.

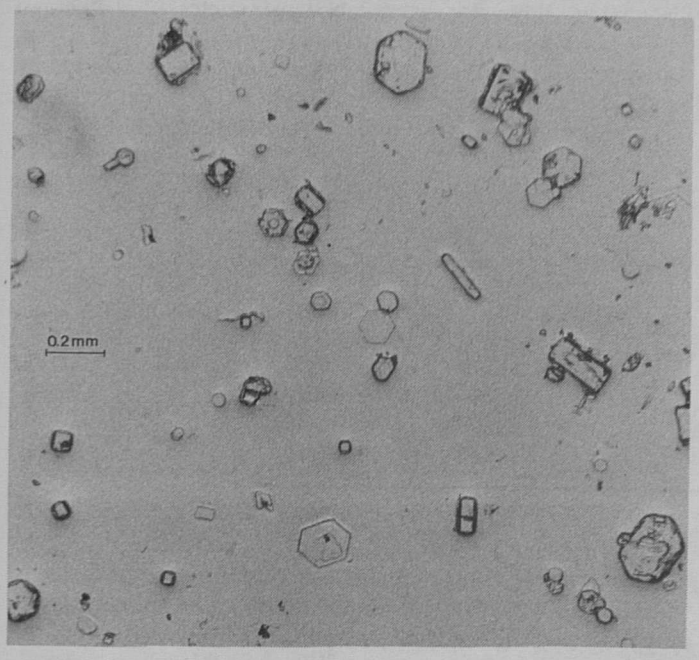

Figure 4. Some crystals that made the halo of figure 2.

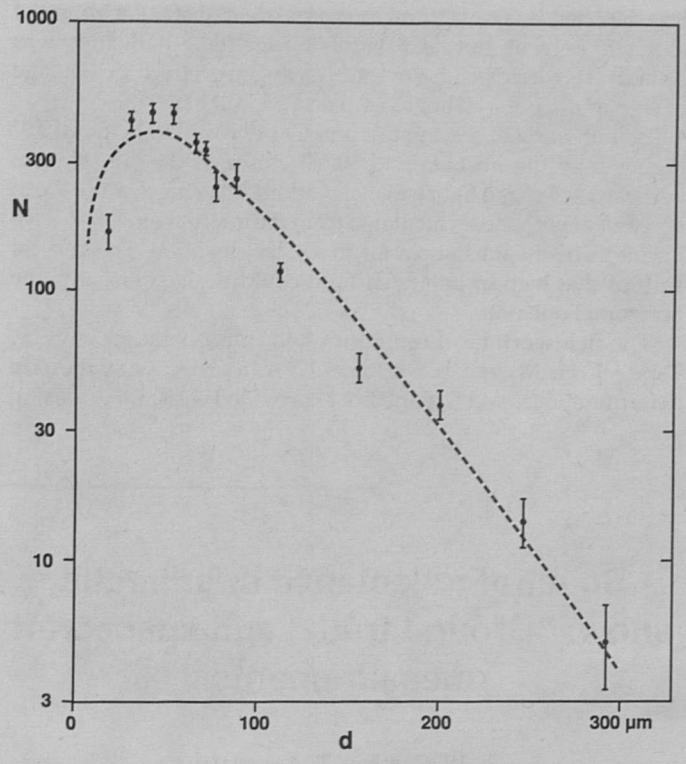

Figure 5. Size distribution of the ice crystals collected during the halo. The size *d* is the crystal hexagon diameter; *N* is the number of crystals per unit size interval. The *dashed line* is a gamma distribution with power one and the observed mean size of 80 micrometers as parameters.

The amount of polarization depends on the slope of the intensity distribution, which is in its turn dependent on the diffraction broadening of the parhelion, caused by the small slit-width of the crystals. Basically, the Q-peak represents a diffraction-broadened delta function. In figure 3, the angular distance $\theta_{1/2}$ between the maximum Q and its half value point is 0.49°.

During the halo display, I made replicas of the falling ice crystals in acrylic spray (see also Tape 1983). Figure 4 shows a picture of some of the replicated crystals in a crystal sample taken 5 minutes after the polarimetric parhelion picture. Since the parhelion remained apparent in front of a nearby black object, the sampled crystals can be considered as halo makers. Mostly they are thin plates lying flat on the spray-covered glass. Figure 5 shows the hexagon size distribution of the crystals, i.e., the number of crystals per unit size interval as a function of hexagon diameter. The observed size distribution resembles closely a gamma distribution with power one and mean size 80 micrometers. The mean thickness of the plates was 30 micrometers. The relation between aspect ratio (crystal length divided by hexagon diameter) and hexagon size could not be determined quantitatively, although it apparently decreased with size (see also Pruppacher and Klett 1978). Assuming the aspect ratio to be constant, a straightforward calculation of $\theta_{1/2}$ of the parhelion Q-peak from the integral of the standard diffraction function for a slit over the observed particle-size gamma distribution predicts $\theta_{1/2}$=0.21°; assuming the thickness to be constant, we get $\theta_{1/2}$=0.26°. Hence, both calculations lead to a $\theta_{1/2}$ of a factor two too small compared with the observed value of 0.49°.

The explanation for this discrepancy can be internal reflection in the crystal, causing a loss of parhelion-generating light in favor of the subparhelion. This loss of parhelion-contributing light becomes increasingly strong for big hexagons when the aspect ratio decreases with size. Hence, there is a predominant contribution of small crystals to the light of the parhelion, and therefore its diffraction broadening is larger than expected from the hexagon size distribution alone. Apparently it leads to an underestimation of a factor two when sizes of parhelion-making crystals are determined optically from the polarization or intensity distribution of this halo. This selection effect is characteristic of the parhelion; a circular 22° halo would not suffer from this.

It is not obvious that high-level crystals have the same size distribution as do low-level ones; the observed gamma distribution may represent just an early stage to be evolved to another distribution with larger sizes. Diffraction-broadened parhelia are indeed rare in the high-level displays of the mid-latitudes; mostly their appearance resembles more that of figure 16 in Können and Tinbergen 1991, with a sharp inner edge. Since, in general, the size distribution of halo-making crystals cannot be determined directly, it is important to know what the optically determined size means. A good parameter for this is the size that contributes most to the intensity. However, to get this figure from the present measurements, we have to multiply the optically determined size obtained with the earlier method (Können and Tinbergen 1991) by a factor of about 0.8. An advantage of this parameter is that it is not very sensitive to the size distribution, at least for gamma distributions with powers up to 5.

The present measurements support our view (Können and Tinbergen 1991) that halo polarimetry is a sensitive tool for detecting birefringent crystals in the terrestrial atmosphere or in the atmospheres of other planets. On the other hand, it turns out that for certain halos, including the parhelion, the optically determined crystal size bears no obvious relationship to the real crystal dimensions in the halo-generating cloud.

At South Pole and Vostok, the polarization of several other types of halo have been recorded. Some findings are as follows:

- A circumzenithal arc, observed simultaneously with the parhe-

lion depicted in figure 2, had an overall degree of polarization of about 20 percent, but near its inner edge the polarization was considerably less because of the birefringence effect. No change of sign of the polarization was observed in that region.

• The 120° parhelion is in horizontally polarized light about 0.2° higher over the horizon and 0.05° closer to the sun than in vertically polarized light (solar elevation 23°). These values are in agreement with those calculated from the internal reflection laws for birefringent substances for this solar elevation. The vertical shift of that halo in polarized light could be seen visually; the horizontal one not.

The fieldwork has been performed in cooperation with W. Tape. J. H. M. van Lieverloo, KIWA, assisted with the size determinations, and R. S. Le Poole provided assistance in using the Leiden University Astroscan densitometer. J. Tinbergen advised on the polarimetry; the camera was rebuilt by H. Deen, Kapteyn Observatory, Roden. This research was supported by National Science Foundation grant DPP 88-16515 and partly by the Netherlands Organization for Scientific Research.

References

Können, G. P. and J. Tinbergen. 1991. Polarimetry of a 22° halo. *Applied Optics*, 30:3,382-3,400.

Tape, W. 1983. Some ice crystals that made halos. *Journal of Optical Society of America*, 73:1,641-1,645.

Pruppacher, H. R. and J. D. Klett. 1978. *Microphysics of clouds and precipitation*. Dordrecht, Netherlands: Nijhoff.

Spectral reflectance of antarctic snow: "Ground truth" and spacecraft measurements

R. W. Carlson, T. Arakelian, and W. D. Smythe

Jet Propulsion Laboratory
California Institute of Technology
Pasadena, California 91109

The cold climate of Antarctica is a result of the high reflectance of snow and of the corresponding small amount of energy that is absorbed from the incident sunlight. The energy-absorption rate depends on such variables as grain size, impurities, and incidence angle, as well as on the wavelength of the incident light. In the visible region, ice is highly nonabsorbing, but becomes a strong absorber in the infrared because of molecular vibrational transitions. To understand energy-absorption rates, it is important to investigate the optical properties of antarctic snow over an extended wavelength range—from the ultraviolet to the infrared. Furthermore, for climatological purposes, it is important to understand these properties throughout the antarctic continent. This can only be accomplished by a program of aircraft or satellite remote sensing measurements in conjunction with locally established "ground truth."

In this article, we briefly describe field measurements of the spectral reflectance of snow at two sites, and compare the optically derived snow grain sizes with photographic measurements of the surface grains. These "ground-truth" data are then used to corroborate spacecraft remote-sensing measurements, thereby extending our localized measurements to continental scales.

The field measurements were obtained in December 1989 at the Amundsen-Scott South Pole Station and in December 1991 at the Vostok Station (78° S 107° E). The field instrumentation consists of a portable diffraction-grating spectrometer mounted on a 1-meter-long goniometric arm. This arm swings in a vertical plane, allowing spectral measurements to be obtained over nearly a 180-degree range of emission angles . We obtained complete spectra for nadir viewing with a variety of solar zenith angles. The goniometric measurements were obtained for a variety of individual wavelengths, both inside and outside of water absorption bands. Here we discuss only a few of the spectra and none of the goniometric measurements.

The experimental procedure was used to measure the spectral radiance for a chosen area of snow, which receives sunlight as well as diffuse radiation from the sky. We then block the sunlight and measure the radiance for only incident skylight. The procedure is repeated using calibrated diffuse reflectance standards such as Halon and sulfur surfaces. With this set of measurements, we obtain the bidirectional reflectance of the snow surface and the diffuse-directional reflectance appropriate to skylight. We also find the relative contribution of diffuse skylight to the total radiance, which is appreciable in the ultraviolet and blue regions of the spectrum.

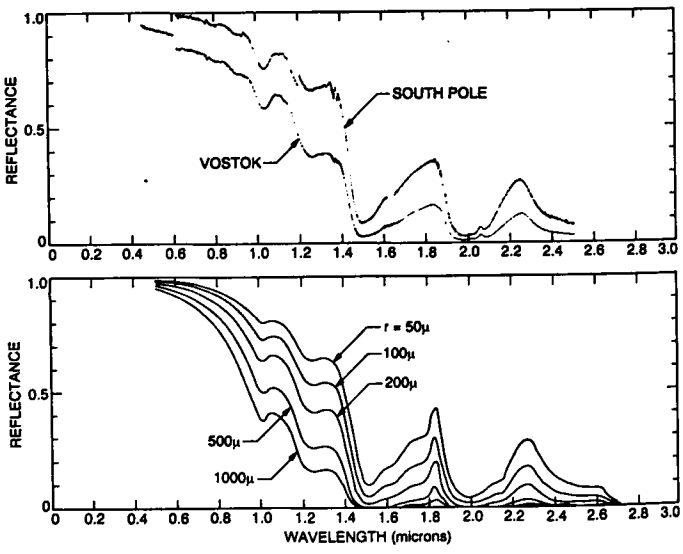

Figure 1. Spectral reflectance of snow. The upper panel is directional-directional reflectance spectra measured at the South Pole and Vostok stations. For both sites, the incidence angle was about 68 degrees and the emission angle was zero, relative to the vertical. The lower panel shows theoretical directional (60 degree) - hemispherical reflectances, computed for varying grain radii by Wiscombe and Warren (1981). A comparison indicates that snow particles at South Pole and Vostok are about 50 and 200 microns in radius, respectively.